# FIELD RECONSTRUCTION BY PASSBAND FREQUENCY MEASUREMENT AT THE ROSSENDORF SRF-GUN CAVITY

A. Arnold[#], H. Buettig, D. Janssen, G. Staats, J. Teichert, FZD, Dresden, Germany

*Abstract*

In this paper a method is presented that provides the field profile of a closed superconducting cavity only by measuring its passband frequencies with the applied RF coupling probes. This opens the possibility to estimate field deformations that are caused by the preload of the cavity tuner and its tuning during operation.

The method was tested at the 3.5 cell Rossendorf SRF gun cavity [1] and a comparison between the measured and predicted field distribution demonstrates the accuracy within a range of 2%.

## INTRODUCTION

In contrast to the TESLA cavities the shapes and the mechanical stiffness of the four SRF-Gun cells differ from each other. Furthermore the axis field to achieve a "flat" surface field over all cells is distributed to 60% in the first and 100% in the TESLA like cells, respectively (cp. Fig. 2 & ref. [2]). Due to the different mechanical properties one tuner for the half cell and one for the three TESLA cells are assembled. Both of them are equipped to adjust the frequency of the cavity during clean room assembling and later during operation. But they also affect the field distribution. Hence, it is very important to determine their influence on the fundamental mode inside the cleaned and closed cavity in order to achieve the needed specifications. The method presented in this paper opens this ability.
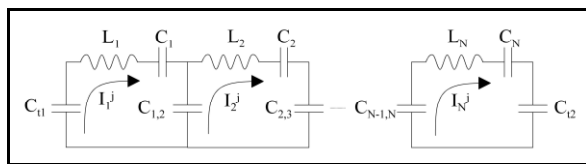
## EQUIVALENT CIRCUIT OF A CELL COUPLED CAVITY



Fig. 1: equivalent circuit of a cell coupled cavity.

For the $TM_{010}$ fundamental modes, an rf resonator can be described by a capacitively coupled resonant circuit with mesh currents that are proportional to the field strength in the different cavity cells (Fig. 1). Based on the Kirchhoff's current law and the normalizations given in eq. 1 the equivalent circuit is described by an eigenvalue problem as shown in eq. 3 and ref. [1], respectively.

$$\frac{1}{LC} = \omega_0^2, \quad \omega_0 = 2\pi \cdot 1275.95 Mhz, \quad \frac{C}{C_{n,n+1}} = k_{n,n+1},$$

$$\frac{C}{C_n} = 1 + \delta_n, \quad \frac{C}{C_{t_m}} = \gamma_m, \quad L_n = L, \quad n = 1...N, \quad m = 1,2 \tag{1}$$

The matrix **A** characterizes the initial state of the cavity. The eigenvector $I^i$ presents the field distribution of the $i^{th}$ fundamental mode and $\lambda_i$ is the corresponding normalized frequency. In general the normalization doesn't matters but it is wise to use the frequency $\omega_0$ of a single cell TESLA cavity.

In order to calculate the elements of the matrix, a complete measurement of the fundamental mode field distributions and its passband frequencies is sufficient. **A** is then fully described by eq. 2.

$$\mathbf{A} = \mathbf{J} \circ \mathbf{D} \circ \mathbf{J}^{-1}$$

$$\mathbf{J} = \begin{bmatrix} I_1^1 & \cdots & I_1^i \\ \vdots & \ddots & \vdots \\ I_N^1 & \cdots & I_N^i \end{bmatrix}, \quad \mathbf{D} = \mathbf{E} \circ \begin{pmatrix} \lambda_1 \\ \vdots \\ \lambda_i \end{pmatrix} \tag{2}$$
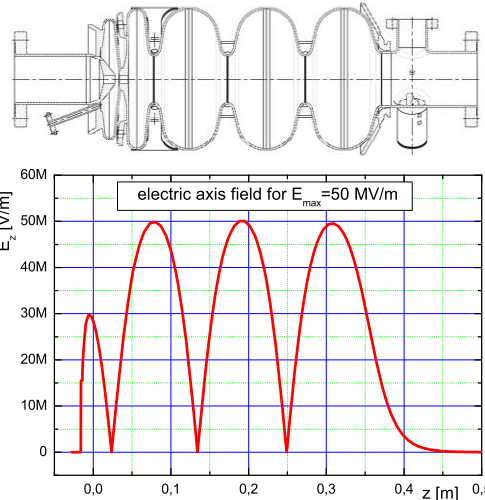


Fig. 2: cavity shape and its corresponding axis field distribution for flat π-mode surface field.

$$\begin{bmatrix} 1+\delta_1+k_{1,2}+\gamma_1 & -k_{1,2} & 0 & \cdots & 0 \\ -k_{2,1} & 1+\delta_2+k_{2,1}+k_{2,3} & -k_{2,3} & \cdots & 0 \\ 0 & -k_{3,2} & 1+\delta_3+k_{3,2}+k_{3,4} & \cdots & \vdots \\ \vdots & \vdots & \vdots & \ddots & -k_{N-1,N} \\ 0 & 0 & \cdots & -k_{N,N-1} & 1+\delta_N+k_{N-1,N}+\gamma_2 \end{bmatrix}_{\mathbf{A}} \circ \begin{pmatrix} I_1 \\ I_2 \\ \vdots \\ \vdots \\ I_N \end{pmatrix}_i = \underbrace{\left(\frac{\omega_i^2}{\omega_0^2}\right)}_{\lambda_i} \circ \begin{pmatrix} I_1 \\ I_2 \\ \vdots \\ \vdots \\ I_N \end{pmatrix}_i \tag{3}$$

$$\underbrace{\phantom{xxx}}_{\mathbf{I}^i} \qquad \underbrace{\phantom{xxx}}_{\mathbf{I}^i}$$

# a.arnold@fzd.de

## RECONSTRUCTION OF THE FIELD DISTRIBUTION

In order to reconstruct the cavity state at an arbitrary moment based on one passband measurement, it is necessary to know the initial state of the matrix **A** before. Then the modification to the moment of interest can be described by addition of a matrix **M** (cp. eq. 4). The elements $m_{i,j}$ of this matrix will be calculated by resolving the system of eigenvalue equations based on the measured passband frequencies $\lambda_i$' (eq. 5). Due to the limitation of N eigenvalues only the diagonal elements $m_{11...NN}$ of the matrix **M** can be solved. This is justified because the tuning within a small range only affects the capacitor $C_n$ of each cell in the equivalent circuit.

$$\left(\mathbf{A}+\mathbf{M}\right)\circ\mathbf{I}^{i'}=\underset{\substack{\text{measured}\\\text{passband}\\\text{frequencies}}}{\lambda_i'}\circ\underset{\substack{\text{field distribution}\\\text{of interest}}}{\mathbf{I}^{i'}}$$

$$\mathbf{M}=\begin{bmatrix} m_{11} & m_{12} & 0 & 0 \\ m_{21} & m_{22} & \ddots & 0 \\ 0 & \ddots & \ddots & m_{N-1,N} \\ 0 & 0 & m_{N,N-1} & m_{N,N} \end{bmatrix} \qquad (4)$$

The cell to cell coupling is untouched and thus the elements of the secondary diagonals are negligible. Using this approximation a simplified calculation of the elements is possible.

$$\det\left(\underbrace{\mathbf{A}+\mathbf{M}}_{\mathbf{A}'}-\lambda_i'\mathbf{E}\right)=0;\quad i=1...N \qquad (5)$$

In combination with the transformation matrix **M**, the field distribution of all fundamental modes are easily predictable by calculating the eigenvectors $\mathbf{I}^{i'}$ by solving the matrix equation 6.

$$\left(\mathbf{A}'-\lambda_i'\mathbf{E}\right)\mathbf{I}^{i'}=\mathbf{0};\quad i=1...N \qquad (6)$$

## VERIFICATION BY MEASUREMENTS

The Rossendorf SRF-Gun cavity consists of 4 cells, which leads to 4x4 matrices and column vectors with 4 elements. To verify the algorithm described above, two complete measurements of two different cavity states will be compared.

$$\mathbf{J}=\begin{bmatrix} 100 & -53.4 & 64.4 & -64.4 \\ 60.4 & 17.4 & -75.2 & 100 \\ 24.6 & 100 & -17.5 & -92.7 \\ \underset{1/4\pi}{0} & \underset{2/4\pi}{58.3} & \underset{3/4\pi}{100} & \underset{4/4\pi}{90.7} \end{bmatrix}[\%] \qquad (7)$$

In the first step the matrix **A** of the initial cavity state is calculated using eq. 2. The required field distributions of the fundamental modes shown in eq. 7 are measured using a bead pull measuring station. Its corresponding frequencies are:

$$\vec{\lambda}=\begin{pmatrix}\lambda_1\\\lambda_2\\\lambda_3\\\lambda_4\end{pmatrix}=\frac{1}{f_0^2}\cdot\overrightarrow{f^2}=\left[\left(\frac{1}{1275.95^2}\right)\cdot\begin{pmatrix}1265.918^2\\1280.749^2\\1292.999^2\\1298.387^2\end{pmatrix}\right] \qquad (8)$$

Both equations lead to the matrix of interest:

$$\mathbf{A}=\begin{bmatrix} 0.998906 & -0.02393 & -0.000423 & -0.000035 \\ -0.016309 & 1.015445 & -0.01016 & 0.000114 \\ -0.00085 & -0.010929 & 1.014697 & -0.009800 \\ 0.00157 & 0.001341 & -0.009692 & 1.025205 \end{bmatrix} \qquad (9)$$

In the second step the measured passband frequencies (cp. eq. 10) of the investigated cavity state will be used to solve the system of four eigenvalue equations (cp. eq. 11) in order to find the diagonal elements of transformation matrix **M**.

$$\vec{\lambda}'=\begin{pmatrix}\lambda_1'\\\lambda_2'\\\lambda_3'\\\lambda_4'\end{pmatrix}=\frac{1}{f_0^2}\cdot\overrightarrow{f^{2'}}=\left(\frac{1}{1275.95^2}\right)\cdot\begin{pmatrix}1265.760^2\\1281.030^2\\1293.057^2\\1298.535^2\end{pmatrix} \qquad (10)$$

$$\begin{aligned}(1)&\left|\mathbf{A}_{4x4}+\mathbf{M}_{4x4}-\lambda_1'\cdot\mathbf{E}_{4x4}\right|=0\\(2)&\left|\mathbf{A}_{4x4}+\mathbf{M}_{4x4}-\lambda_2'\cdot\mathbf{E}_{4x4}\right|=0\\(3)&\left|\mathbf{A}_{4x4}+\mathbf{M}_{4x4}-\lambda_3'\cdot\mathbf{E}_{4x4}\right|=0\\(4)&\left|\mathbf{A}_{4x4}+\mathbf{M}_{4x4}-\lambda_4'\cdot\mathbf{E}_{4x4}\right|=0\end{aligned} \qquad (11)$$

A numerical algorithm implemented in MathCad© is used to solve the elements $m_{11}$ to $m_{NN}$ and matrix **A'** is expressed by eq. 12.

$$\mathbf{A}'=\mathbf{A}+\underbrace{\begin{bmatrix} -0.00042617 & 0 & 0 & 0 \\ 0 & -0.00003926 & 0 & 0 \\ 0 & 0 & 0.0006648 & 0 \\ 0 & 0 & 0 & 0.0003253 \end{bmatrix}}_{\mathbf{M}} \qquad (12)$$

| measured field profile in % | | | | calculated field profile in % | | | |
|---|---|---|---|---|---|---|---|
| 100 | -52.6 | 67.7 | -63.8 | 100 | -53.1 | 66.0 | -63.3 |
| 58.5 | 18.2 | -77.7 | 100 | 59.7 | 19.2 | -78.5 | 100 |
| 24.7 | 100 | -15.9 | -97.2 | 23.5 | 100 | -15.3 | -97.3 |
| 0 | 58.1 | 100 | 95.9 | -0.2 | 58.5 | 100 | 96.0 |
| 1/4π | 2/4π | 3/4π | 4/4π | 1/4π | 2/4π | 3/4π | 4/4π |

Fig. 3: comparison of the measured & calculated field profiles of all four modes, starting with the ½ cell.

The field distribution calculated out of the eigenvectors of the new matrix **A'** will be finally compared to the results of an additional bead pull measurement that was done afterwards. As shown in Fig. 3, the calculated fields as well as the measured real fields coincide within small differences of less than 2% for all modes. In particular the accuracy of the acceleration mode is better than 1%.

## CONSIDERATION OF DIFFERENT FEQUENCY SHIFTS

There are at least three sources that affect a shifting of the passband frequencies after the last possible bead pull measurement. The main effect is caused by the cooldown shrinking of the cavity that can be considered by eq. 13.

$$f_{cold} = \frac{f_0}{(1+\alpha)}; \quad \begin{array}{l} \alpha...\text{coefficient of thermal expansion} \\ \alpha(300\text{K-2K}) = \Delta l/l = -1.47 \cdot 10^{-3} \end{array} \quad (13)$$

The second shift is induced by the different relative static permittivity $\varepsilon_r$ of an evacuated cavity compared to the air filled cavity during the last field measurement (cp. eq. 14).

$$f_{vacuum} = \frac{f_{Air}}{\sqrt{\varepsilon_{r,Air}}}; \quad \varepsilon_{r,Air} = 1.00059 \quad (14)$$

These both effects are physically well defined, but the frequency variation caused by chemical etching has to be approximated by numerical simulation with an equal material removal. Due to the small reduction of about 20µm during the final standard treatment, the elements of the second diagonals are assumed to be unchanged and thus the field reconstruction introduced above is useable.

The consideration of all three frequency shifts can be done by its addition to the initial passband of the last bead pull measurement. This is reasonable because the described cavity changes are uniformly and the field distribution is untouched. Based on the modified passband, a matrix **A**$_{cryo}$ projected into cleaned & cryogen conditions is calculated to replace the original matrix A introduced in chapter two.

To show a numerical example, the passband given in eq.10 is modified as follows:

$$\vec{f}_{cryogen} \atop [MHz] = \underbrace{\begin{pmatrix} 1265.760 \\ 1281.030 \\ 1293.057 \\ 1298.535 \end{pmatrix}}_{\text{passband of eq.10}} + \underbrace{\begin{pmatrix} 1.863 \\ 1.896 \\ 1.903 \\ 1.912 \end{pmatrix}}_{\text{cooldown}} + \underbrace{\begin{pmatrix} 0.373 \\ 0.378 \\ 0.381 \\ 0.383 \end{pmatrix}}_{\text{vacuum}} + \underbrace{\begin{pmatrix} -0.261 \\ -0.264 \\ -0.232 \\ -0.217 \end{pmatrix}}_{\text{simulated etching}}$$

$$\vec{f}_{cryogen} \atop [MHz] = \begin{pmatrix} 1267.735 \\ 1283.040 \\ 1295.109 \\ 1300.613 \end{pmatrix} \quad (15)$$

The frequency shift caused by etching is approximated using a Superfish© simulation with a homogeneous material removal of 20µm.

The new matrix **A**$_{cryo}$ which describes the initial state of the cleaned, cold and evacuated but untuned cavity is calculated using eq. 16 and the measured field distributions of Fig. 3. By means of this new starting point the field modifications caused by clean room assembling and frequency tuning during operation can be estimated by one single passband measurement.

$$\mathbf{A}_{cryo} = \begin{bmatrix} 1.001691 & -0.024567 & -0.000600 & 0.000153 \\ -0.016022 & 1.01876 & -0.010007 & 0.000326 \\ -0.001100 & -0.011282 & 1.01837 & -0.009912 \\ 0.001557 & 0.001422 & -0.009681 & 1.028771 \end{bmatrix} \quad (16)$$

## CONCLUSION

The method presented in this paper is convenient to calculate the field distribution of a cold and closed cavity only by measuring its passband frequencies with the applied rf field probes. But the limitation on N parameters to resolve the equations, leads to its limited ambit. The tuning range has to be small compared to the frequency and the material removal caused by etching needs to be negligible. In both cases the cell to cell coupling and the elements of the secondary diagonals are approximately unchanged.

Another uncertainty is the frequency shift caused by chemical treatment. In difference to the Superfish© simulation, the real removal rate at the inner surface is not homogenous. This leads to an unknown shift of each passband frequency and to an unknown error that has to be quantified by future measurements done after chemical etching.

## ACKNOWLEDGEMENT

## REFERENCES

[1] A. Arnold, et al., "Development of a Superconduc-ting Radio Frequency Photo Electron Injektor", Nucl. Instr. and Meth. A 577 (2007) 440.

[2] A. Arnold, et al., "First RF Measurements at 3.5 Cell SRF-Photo-Gun Cavitiy in Rossendorf", Proc. FEL 2006, Berlin, Germany, p. 567.

[3] C. Cooper., "Single Iteration Tuning for Multicell RF Cavities for Cornell ERL", REU research reports, Cornell University, NY, USA, 2003.